Journal of Materials Chemistry C

PAPER

View Article Online
View Journal

Cite this: DOI: 10.1039/c8tc04872j

Amine additive reactions induced by the soft Lewis acidity of Pb^{2+} in halide perovskites. Part II: impacts of amido Pb impurities in methylammonium lead triiodide thin films†

Ross A. Kerner, [a] Tracy H. Schloemer, [b] Philip Schulz,[cd] Joseph J. Berry, [c] Jeffrey Schwartz,[e] Alan Sellinger [bcf] and Barry P. Rand *[ag]

Received 26th September 2018,
Accepted 15th November 2018

DOI: 10.1039/c8tc04872j

rsc.li/materials-c

The performance of lead halide perovskite optoelectronic devices continues to improve, yet the efficiencies are still well below the radiative limit. To approach the radiative limit, detailed understanding of impurities/defects and precise control over their concentrations are required. In Part I, we demonstrated that the soft Lewis acidity of Pb^{2+} induces a chemical reaction between PbI_2 and aliphatic amines producing Pb-alkylamide bonds which can be subsequently incorporated into thin films. Here, we investigate the consequences of these impurities in methylammonium lead triiodide ($MAPbI_3$) thin films. In particular, we link Pb–alkylamide impurities to an extrinsic degradation pathway resulting in Pb^0 formation. The proposed mechanisms proceeds *via* β-C–H proton transfer reactions of the amido Pb species. Metallic Pb^+/Pb^0 defects acting as non-radiative recombination centers may limit the performance of many perovskite layers. However, optimal concentrations of Pb–methylamide impurities in sub-stoichiometric (slight excess of PbI_2) $MAPbI_3$ films passivate Pb^0 defect formation, shown here to simultaneously correlate to improvements in photoluminescence lifetime. These results elucidate the beneficial properties of Pb–amide impurities in low concentrations and the sensitivity of halide perovskite materials to extrinsic defect chemistry.

Introduction

Optoelectronic devices (photovoltaics, light emitting diodes, lasers, *etc.*) based on metal halide perovskite semiconductors have realized high performance in a relatively short period of time.[1–5] The electronic properties of perovskites seem to be unaffected by intrinsic defects within the bulk, yet reported quantum efficiencies are quite low, indicating that extrinsic impurities within the bulk, at surfaces, and at interfaces restrict performance.[3,6] Progress in record perovskite efficiencies is slowing near 22%; a trend converged upon by all polycrystalline photovoltaic technologies such as CIGS and CdTe.[7] This value lies well below the radiative recombination limited efficiency of over 30% predicted by Shockley-Quiesser detailed balance for AM1.5G simulated solar illumination and a bandgap of approximately 1.5–1.6 eV.[8] Thus, strict management of impurities, defects, and interfaces is necessary to advance perovskite devices toward their radiative limit.

In a previous study, we demonstrated that a reaction between PbI_2 and aliphatic amines can produce Pb–alkylamide impurities due to the soft Lewis acidity of Pb^{2+}.[9] This is an important consideration as amines become increasingly more common in perovskite processing.[1,2,10–14] It thus appears that ink formulations with an excess of PbI_2 are especially prone to alkylamide (generally referred to as amide hereafter) formation and, under mild reaction conditions, amide groups can be subsequently incorporated into perovskite thin films in concentrations large enough to resolve with X-ray photoelectron spectroscopy (XPS).[9] The full extent of the consequences of Pb–amide impurities as well as their location (*i.e.* surface *versus* bulk) in perovskite films are yet to be determined. However, processes utilizing amines resulting in improvements of photoluminescence (PL) properties and device efficiencies suggest that amides may be involved in defect passivation.[1,2,9–14]

[a] Department of Electrical Engineering, Princeton University, Princeton, New Jersey 08544, USA. E-mail: brand@princeton.edu
[b] Department of Chemistry, Colorado School of Mines, Golden, Colorado 80401, USA
[c] National Renewable Energy Laboratory, Golden, Colorado 80401, USA
[d] CNRS, Institut Photovoltaïque d'Ile de France (IPVF), UMR 9006, Palaiseau, France
[e] Department of Chemistry, Princeton University, Princeton, New Jersey 08544, USA
[f] Materials Science Program, Colorado School of Mines, Golden, Colorado 80401, USA
[g] Andlinger Center for Energy and the Environment, Princeton University, Princeton, New Jersey 08544, USA

† Electronic supplementary information (ESI) available. See DOI: 10.1039/c8tc04872j

In this follow up study, we begin with an investigation of the reactivity and stability of amide groups in PbI_2 resulting from amine/amide reactions in solution, vapor phase, and solid-state. Notably, we find that PbI_2 exposed to aliphatic amines correlates to the rapid development of Pb^0 under X-ray and visible light illumination in ultra-high vacuum (UHV) conditions (*e.g.* during XPS) relative to controls. Since we have shown that amine exposure produces Pb–amide bonds, it is assumed that these organometallic species facilitate reduction of Pb^{2+} to Pb^0 through proton transfer reactions.

From these observations, we conclude that exposure of PbI_2 to amines can result in amide formation which then facilitates an extrinsic decomposition pathway to Pb^0.

We extend the study to investigate the stability of methylammonium lead triiodide ($MAPbI_3$) formulations that are more relevant for halide perovskite optoelectronics. We discover that sub-stoichiometric solutions ($MAI:PbI_2$ precursor ratios <1) producing films that are mixtures of PbI_2 and $MAPbI_3$ phases show greatly accelerated Pb^0 formation in XPS while phase pure PbI_2 and $MAPbI_3$ controls are relatively robust. Based on the observation that amine exposure leads to Pb^0, we hypothesize that irradiation induced reactions at the $PbI_2/MAPbI_3$ phase boundary release methylamine which is converted to methylamide by excess PbI_2 leading to the Pb^0 formation. Thus, the implications of the amine/amide reaction can be extended to "self-exposure" as organoammonium containing perovskites decompose into PbI_2 and the respective amine.

Finally, we highlight the beneficial aspects of low concentrations of Pb–amide species by showing that methylamine additives in near-stoichiometric inks react with the excess PbI_2. However, in contrast to pristine PbI_2, the intentional incorporation of optimal concentrations of Pb–methylamide impurities in $MAPbI_3$ leads to improved stability during XPS measurements and negligible Pb^0 formation. The passivating capabilities of methylamide are also revealed by improvements in PL characteristics. Photoluminescence properties are known to be dominated by surface defects which suggests that low concentrations of Pb–amides primarily attach at perovskite crystal surfaces.[6] These results are an important step in identifying extrinsic impurities in perovskites and engineering strategies that maximize the passivating properties of intentional or unintentional incorporation of Pb–amide impurities.

Results and discussion

Pb–Amide degradation to Pb^0

Depicted in Fig. 1a–d are initial XPS measurements (black traces) of the Pb $4f_{7/2}$ peak of thin films of a PbI_2 control, PbI_2 reacted with methylamine in solution with anhydrous *N*,*N*-dimethylformamide, a solid PbI_2 film exposed to methylamine vapor at room temperature, and a solid-state thin film heterojunction of PbI_2/linear polyethylenimine (PEI), respectively, in addition to a scan after 15 minutes of continuous X-ray exposure (red traces). The corresponding I 3d, N 1s, C 1s, and O 1s spectra are in Fig. S1–S3 (ESI†). Little to no oxygen was detected in any of the samples except the PbI_2/PEI sample due to the terminating hydroxyl groups in PEI. It is clear from Fig. 1a–d that, relative to the control (Fig. 1a), exposure of PbI_2 to amines at any point during the fabrication process results in the accelerated reduction of Pb^{2+} cations ($4f_{7/2}$ BE $\approx$ 138–139 eV) to Pb^0 ($4f_{7/2}$ BE $\approx$ 136.8 eV). In addition, X-rays were not required; illumination from the XPS analysis chamber light was also effective at inducing Pb^0 (Fig. S4, ESI†). The formation of Pb^0 in these samples correlates to the presence of a low BE feature at approximately 401 eV in the N 1s spectra of the PbI_2 exposed to amines during the processing (Fig. S1–S3, ESI†).[9] Recently, Ramadan *et al.* observed, in addition to the methylammonium peak at $\approx$402.6 eV, a strong N 1s XPS peak at 401.2 eV in $MAPbI_3$ films that were processed from an ACN/methylamine solvent system.[15] The presence of the peak at 401.2 eV also correlated with a significant amount of Pb^0 signal at BE $\approx$ 137 eV.[15]

Metallic Pb^0 defects in perovskite films have previously been observed to form *in situ* during XPS due to X-ray or visible light irradiation.[16–18] The reaction mechanism is attributed to photolysis of the perovskite dissociating Pb–halide bonds as shown for $MAPbI_3$ in eqn (1)–(3):[16–18]

$$MAPbI_3 \xrightarrow{h\nu} I_2 + MAI + Pb^0 \quad (1)$$

$$MAPbI_3 \xrightarrow{h\nu} HI + CH_3NH_2 + PbI_2 \quad (2)$$

$$PbI_2 \xrightarrow{h\nu} I_2 + Pb^0 \quad (3)$$

Eqn (1) shows photolysis of the halide directly from the $MAPbI_3$ phase. Eqn (2) conveys the initial decomposition of $MAPbI_3$ into PbI_2, losing volatile HI and methylamine, followed by photolysis of PbI_2 leading to the reduction of Pb^{2+} (eqn (3)). However, gas effusion measurements identifying H_2, CH_2, NH_2, NH_3, and CH_3I products evolving from $MAPbI_3$ films during decomposition in vacuum indicate that eqn (1)–(3) are not a comprehensive set of degradation pathways.[19,20]

The relative changes in the peak intensities for the samples in Fig. 1 are quite small, though, the largest losses appear to be of C and N (Fig. S1 and S2, ESI†). This is supported by percent changes in peak areas before and after degradation which are quantified in Table S1 (ESI†). We hypothesize that the incorporation of organometallic Pb–amide bonds enables extrinsic reaction pathways for Pb^{2+} reduction and offer a plausible mechanism. Under excitation (either thermal, X-rays, photoelectron collision, or visible light illumination) abstraction of the acidified β-C–H proton of the amide ligand by a base may occur (Fig. S5, ESI†). This would result in Pb^0, the Schiff base of the amine, and the conjugate acid of the base. There are two species possible of deprotonating the amide ligand: iodide (Fig. S5a, ESI†) to form HI or a second, adjacent amide (Fig. S5b, ESI†) to reform the amine. Since thermal gravimetric analysis (TGA) of PbI(butylamide) shows the amide groups are completely ejected at temperatures below the onset of iodide loss above 500 °C, we must conclude that the amide species is the thermodynamic base.[9] This is supported by negligible loss in iodide during XPS induced degradation.

These observations lead to two possible reaction pathways forming Pb^0 under different conditions. At high concentrations

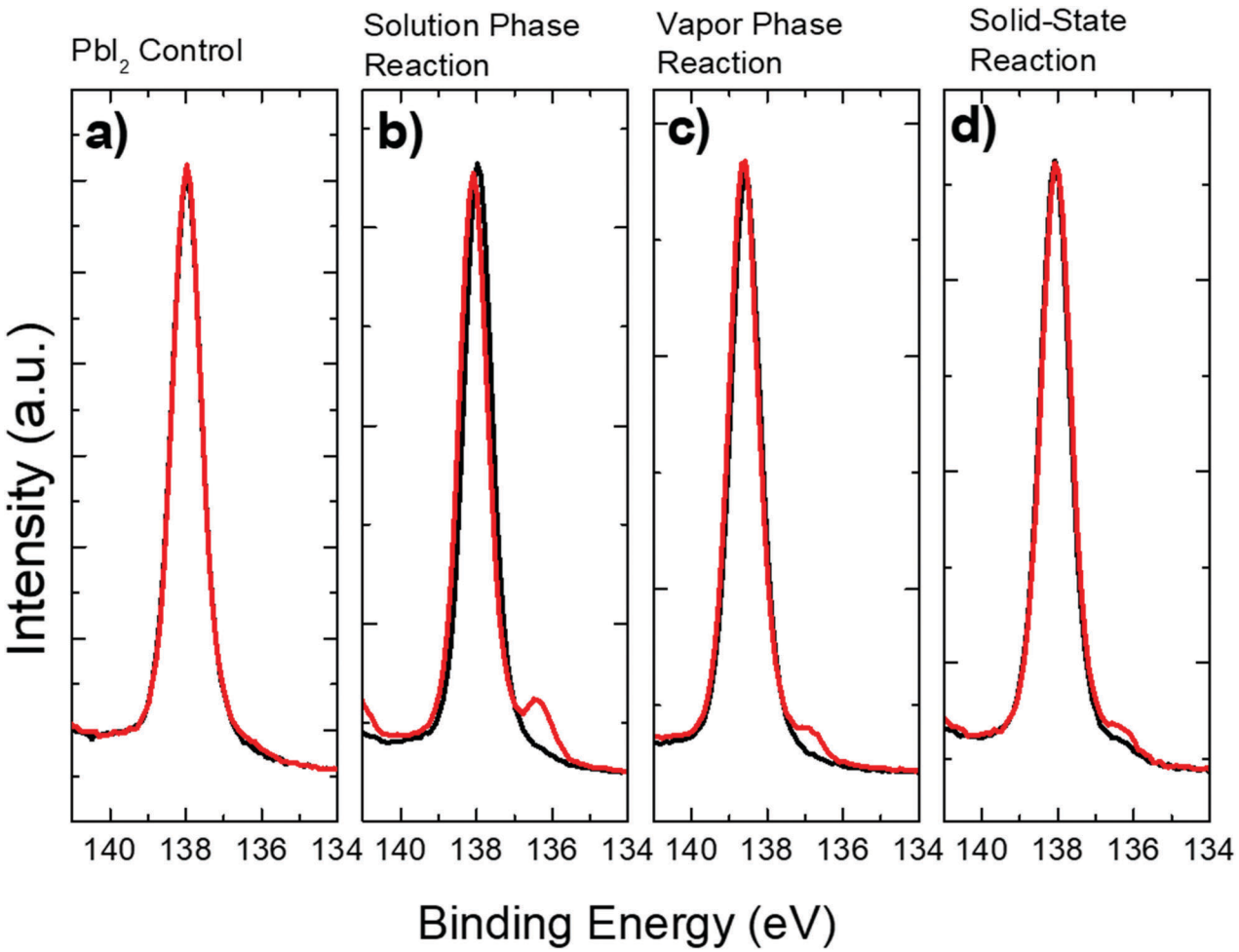

Fig. 1 Pb $4f_{7/2}$ XPS spectra of a thin film of (a) PbI_2 control compared to thin films of PbI_2 reacted with methylamine in (b) solution phase, (c) vapor phase, and (d) at the PbI_2/linear PEI solid-state interface. Black and red curves correspond to initial scans and after 15 minutes of X-ray irradiation, respectively. The presence of Pb–amide species greatly accelerates the development of metallic Pb^0 in UHV.

of Pb–amide, the close proximity of amides allows them to simultaneously act as both the kinetic and thermodynamic base. The rate of Pb^0 formation would depend on the [amide concentration]^2 since two molecules are involved in the reaction step (Fig. S5b, ESI†). At low concentrations of Pb–amide, it is statistically unlikely that two amides will exist on adjacent Pb ions. In this case, the abundant iodide ions act as the kinetic base. The newly formed HI results in relatively mobile protons which can then protonate a distant Pb–amide molecule forming the thermodynamic base (Fig. S5c, ESI†). The rate limiting step at low amide concentrations would undoubtedly be HI formation associated with a larger energy barrier to proton abstraction. This explains the two steps in amide loss in TGA (onset of mass loss at $\approx$230 °C with a second onset at $\approx$330 °C) as a transition in reaction pathway from high to low amide concentration regimes (Fig. S6, ESI†).[9]

Ultimately, when Pb^0 defects are created, comproportionation reactions (eqn (4)) may produce Pb^+ radicals:[21–23]

$$Pb^{2+} + Pb^0 \rightarrow 2Pb^+ \quad (4)$$

Computational studies indicate that intrinsic Pb^+ radicals are stabilized as Pb dimers.[24] Thus, eqn (4) could be written as a cluster of partially reduced Pb ions, but for the purposes of discussion we simply write Pb^+. Defect reaction eqn (4) is evidenced by low temperature electron paramagnetic resonance studies which have directly observed UV induced Pb^+ as a metastable defect in perovskite films.[25] Electron paramagnetic resonance measurements of $MAPbI_3$ also revealed interesting fragmentation of methylammonium into the Schiff base radical cation $[CH_2NH_3]^+$, in support of β-C–H transfer.[25] Furthermore, photoinduced Pb^+ provides a plausible physical origin for the metastable, photoinduced trap states acting as n-type donors that have been applied to phenomenological models of perovskite photoluminescence.[26] The Pb^+ species diffusing into the bulk can be equivalently viewed as iodide vacancies since iodide would need to be consumed to annihilate a metallic Pb^0 atom.

Degradation of sub-stoichiometric films

Much work has been dedicated to optimizing precursor ratios of perovskite inks for which it is generally found that a slight molar excess of PbI_2 relative to the A-site cation precursor salt improves solar cell efficiency.[27] Despite enabling higher initial

device efficiencies, excess PbI_2 has also been linked to decreased material and device stability.[27] Fig. 2a–c show the effect of precursor ratio on the development of Pb^0 during XPS (representative XPS of I 3d, N 1s, C 1s, and O 1s shown in Fig. S7, ESI†). We observed that $PbI_2/MAPbI_3$ thin films spin coated from sub-stoichiometric inks (MAI : PbI_2 precursor ratio <1) accelerated the degradation to form Pb^0 defects. We can interpret the initial BE shifts to higher BE in Fig. 2a and b as a decrease in the work function due to n-type doping resulting from the reaction given by eqn (4). The accelerated degradation rates observed in Fig. 2 contribute to a mechanistic understanding of the lowered stability of sub-stoichiometric compositions.

Our first assumption was that disorder or strain at the $PbI_2/MAPbI_3$ interface may contribute to the accelerated degradation. However, as will be described later, Pb^0 formation does not correlate directly to strain or disorder as measured by X-ray diffraction (XRD). Alternatively, we must invoke the observations made in the previous section where we positively correlated Pb^0 formation to PbI_2/amine exposure and identification of Pb–amide N in XPS. In the case of Fig. 2, since no amines were externally added, the amine must be made available due to self-exposure during photoinduced degradation following eqn (2). The defect tolerance of $MAPbI_3$ and the known existence of phases such as $HPbI_3$ lead us to believe that the $PbI_2/MAPbI_3$ interface is blurred making it more interphasial in nature as depicted in Scheme 1.[16,28] Note that simulated solar illumination was also observed to greatly accelerate the amine to amide conversion.[9] The reactions in Scheme 1 will be strongly affected by heat, voltage bias, and illumination. These reactions provide the mechanism by which $PbI_2/MAPbI_3$ is self-exposed to methylamine *via* deprotonation of the methylammonium cation which can then react further to form methylamides and Pb^+/Pb^0 defects.

Passivation of sub-stoichiometric films by controlled methylamide incorporation

Finally, we systematically investigated the effect of methylamine additives in sub-stoichiometric $MAPbI_3$ precursor inks. As shown in Fig. 3a, methylamine additives in sub-stoichiometric precursor inks (20% excess PbI_2) results in the incorporation of a small, yet measurable amount of amide revealed by the appearance of an increased signal at BE $\approx$ 401 eV that increases over time.[9] In contrast to the control, sub-stoichiometric $MAPbI_3$ films with low

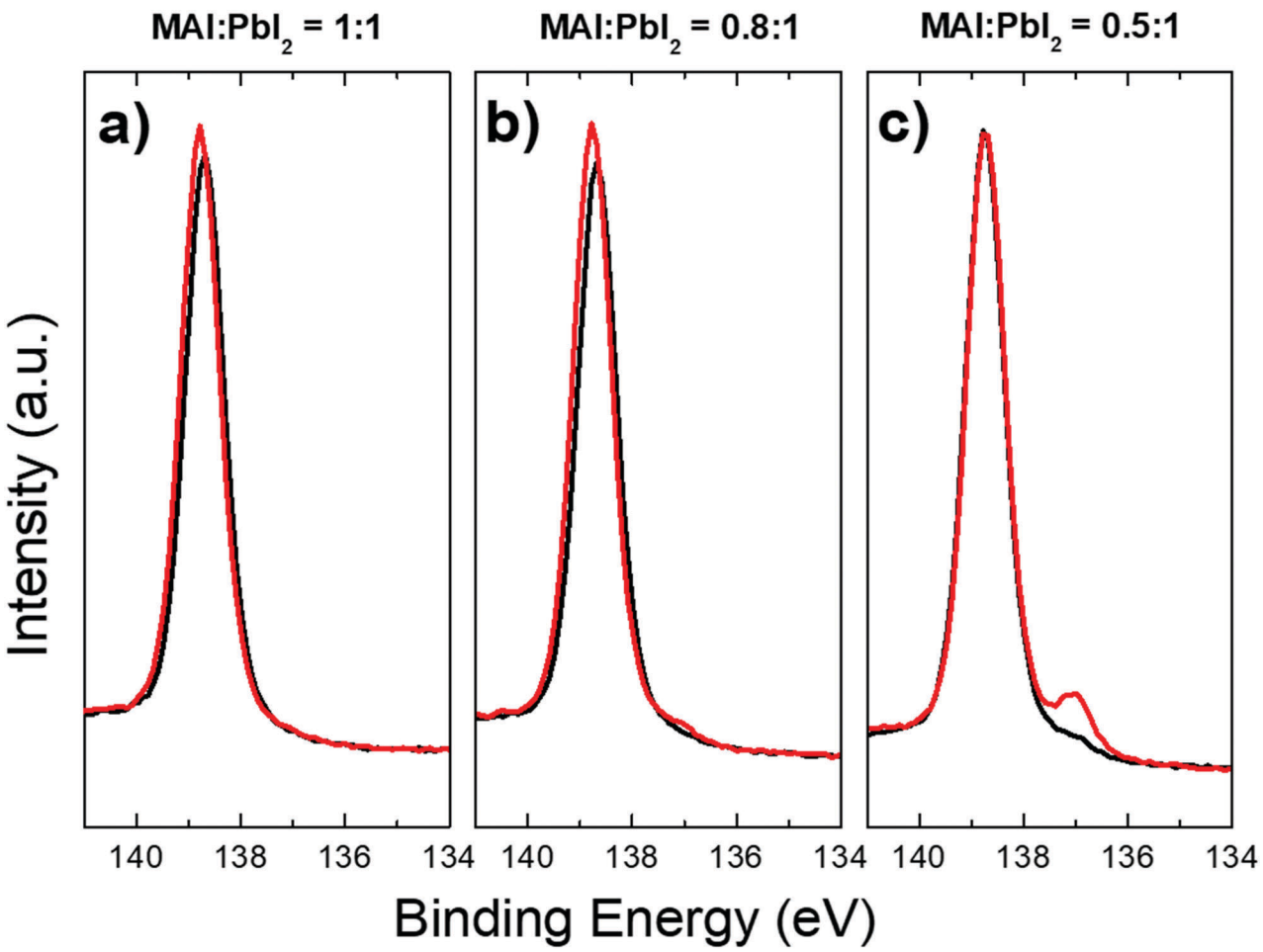

Fig. 2 Pb $4f_{7/2}$ XPS spectra of a thin films cast from solutions with MAI : PbI_2 precursor ratios equal to (a) 1 : 1, (b) 0.8 : 1, and (c) 0.5 : 1. Black and red curves correspond to initial scans and after 25 minutes of simultaneous X-ray irradiation and visible light illumination, respectively. Sub-stoichiometric (PbI_2 rich) precursor formulations destabilize the films w.r.t. Pb^0 formation compared to pristine $MAPbI_3$ and PbI_2 control films.

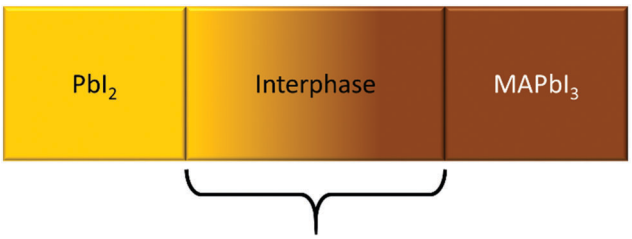

$$(CH_3NH_3)^+I^- + PbI_2 \xrightarrow{h\nu,\ \Delta} CH_3NH_2 + HPbI_3$$

$$2(CH_3NH_2) + 2PbI_2 \xrightarrow{h\nu,\ \Delta} (CH_3NH_3)PbI_3 + PbI(NHCH_3)$$

Scheme 1 Possible reactions giving rise to phases other than PbI_2 and perovskite at the interface of PbI_2 and $MAPbI_3$ grains indicating the boundary may be more accurately described as an interphase.

concentrations of methylamide impurities were more resistant to degradation forming no measurable Pb^0 peak within the same measurement time (Fig. 3b). Solutions reacted for 12–48 h (12 h aging time in Fig. 3b) showed the highest resistance to Pb^0 formation. Thus, intentionally pre-forming methylamide at low concentrations in solution proved to be effective at passivating $MAPbI_3$ films with respect to the degradation observed in Fig. 1 and 2b. There are two reasons we believe methylamide was stable when homogeneously distributed at low concentrations in $MAPbI_3$ whereas, in contrast, it seems that amide groups in PbI_2 are not stable at any concentration. First, low concentrations are necessary to spatially separate amide groups to cut-off the reaction pathway in Fig. S5b (ESI†). Second, PbI_2 can be viewed as the conjugate base of $MAPbI_3$ or $HPbI_3$. Thus, deprotonation by the pathway in Fig. S5a (ESI†) is far more favorable by PbI_2 than for $MAPbI_3$.

The films were characterized by XRD to probe structural changes induced by exposure and reaction with methylamine in solution. The XRD patterns of the sub-stoichiometric controls (no methylamine) in Fig. 3c show the expected PbI_2 (primary reflection $2\theta = 12.66^\circ$) and $MAPbI_3$ (primary reflection $2\theta = 14.08^\circ$) diffraction peaks. In contrast, sub-stoichiometric precursors allowed to react with methylamine for 24 h display peaks that are broadened, have reduced intensity, and are slightly shifted to lower angle (12.60° and 14.04°) compared to the controls. These features indicate that the crystallinity is reduced due to disorder or strain when methylamide is incorporated. The absence of Pb^0 in Fig. 3b rules out disorder/strain as the sole driving force for Pb^0 formation.

Mitigation of Pb^0 defect formation during XPS by the incorporation of low concentrations of methylamide was strongly correlated to PL improvements as well. Time resolved PL (TRPL) of perovskite films encapsulated in PMMA reveals that the carrier lifetime is slightly increased for both stoichiometric and sub-stoichiometric films with methylamine additives (reacted for 24 h) relative to their controls (Fig. S8, ESI†). These results are consistent with numerous literature reports of defect passivation by amine treatments.[2,12–14] We attribute the relatively short lifetimes of the encapsulated films to Pb^+/Pb^0 defects forming *in situ* as we observed due to illumination in UHV (Fig. 2b). Metallic Pb^0 defects, presumably

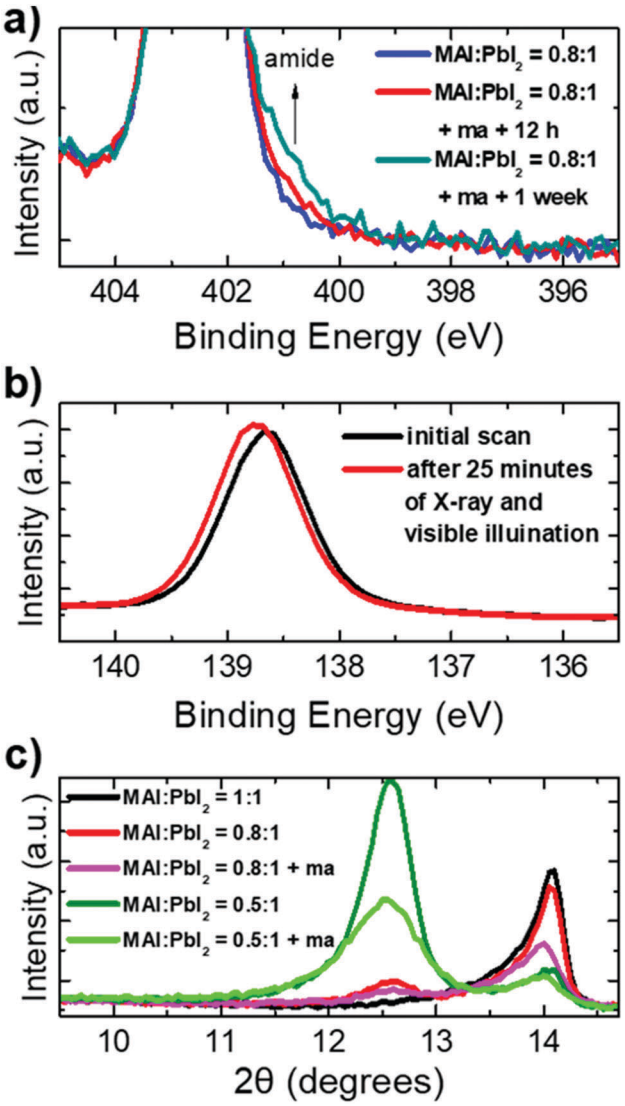

Fig. 3 (a) N 1s XPS of a sub-stoichiometric film (MAI : PbI_2 = 0.8 : 1) with and without methylamine (ma) added to the solution after aging for 12 h and 1 week. (b) Pb $4f_{7/2}$ XPS of MAI : PbI_2 = 0.8 : 1 allowed to react with methylamine in solution for 12 h showing no Pb^0 development. (c) X-ray diffraction patterns of sub-stoichiometric films with and without methylamine added to the precursor solutions.

localized to surfaces, contribute to non-radiative recombination to which we attribute the fast PL decay component.[6] The perovskite layer in contact with Pb^0 will attempt to reach chemical equilibrium with the Pb^0. This drives the comproportionation reaction forward producing Pb^+ donors (eqn (4)), effectively n-type dopes the perovskite, shifts the core level BE to higher values (Fig. 2a–c and 3b), and increases the monomolecular radiative decay rate within the bulk. The longer lifetime of the methylamide containing films corresponds to a reduction in the rate of formation of Pb^0/Pb^+ (Fig. 3a and b). Encapsulated film TRPL lifetimes extracted from a bi-exponential fit before and after aging are given in Table S2 (ESI†) which show that encapsulation preserves the relative improvements in TRPL lifetime for an extended period of time (Fig. S9, ESI†).

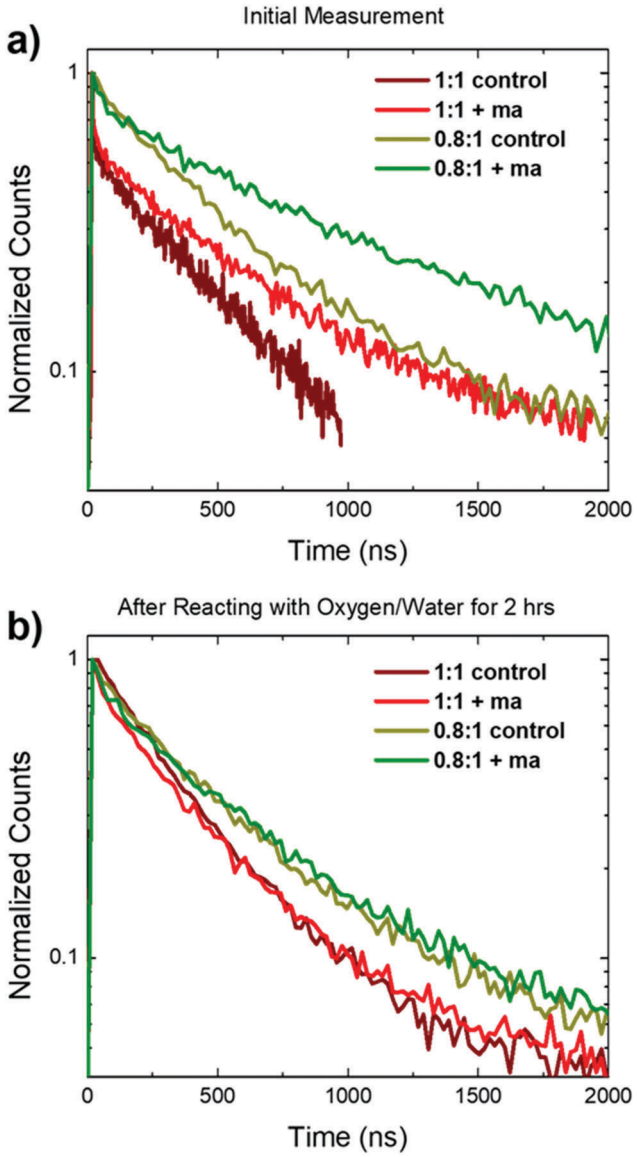

Fig. 4 (a) Initial TRPL measurements in air of the MAI : PbI_2 = 0.8 : 1 with methylamine additive (reacted 24 h) reveals improved optoelectronic properties relative to controls indicating the methylamide incorporation leads to defect passivation. (b) TRPL measurements after allowing the films to photodegrade in atmosphere for 2 h show that they converge to the same performance as the controls.

As shown in Fig. 4a, unencapsulated films also display improved lifetimes for methylamide incorporation relative to the controls. In general, much longer lifetimes were observed for all samples without encapsulation which is attributed mainly to a known reaction where Pb^0 is oxidized by exposure to and/or annealing in the presence of atmospheric water and oxygen.[3,29] Oxidation of Pb^0/Pb^+ both eliminates traps, reducing non-radiative decay, as well as decreases doping increasing the monomolecular lifetime.

Despite reacting with atmosphere, the films containing methylamide initially show a much longer lifetime component than films without methylamine additives (Table S3, ESI†). However, given enough time to react with atmospheric water and oxygen, the methylamide passivated TRPL lifetimes converge on those of their respective controls as shown in Fig. 4b. Reactions with water/oxygen eventually degrades the perovskite layers to similar performance indicating the Pb–methylamide species is reactive with atmosphere. Most importantly, the overarching observation that a small amount of amide species in $MAPbI_3$ correlates to both a lower rate of Pb^0 formation in XPS and simultaneous improvement in PL lifetime strongly suggests that an optimal concentration of amido Pb impurities is involved in passivation of Pb iodide-based perovskites.

Conclusions

An acid–base reaction occurs between PbI_2 and aliphatic amines for which the data overwhelmingly indicate the formation of amido Pb products. We have identified multiple situations in which PbI_2 and perovskite films react with amines and the consequences of subsequent Pb–amide incorporation. Large amounts of Pb–amide species destabilize PbI_2 and $MAPbI_3$, accelerating photoinduced Pb^0 formation *via* proton transfer reactions. However, proper control over the amide concentration for slightly sub-stoichiometric $MAPbI_3$ films both inhibits Pb^0 development during XPS measurements and improves the PL properties. These results exemplify the importance of recognizing reactions that occur in halide perovskite solutions and demonstrate how unintentional chemistry can directly affect the optoelectronic properties of perovskite thin films. The interplay between beneficial and detrimental effects of this impurity and the significant effects on material properties highlight the need for a more detailed understanding and awareness of potential extrinsic impurities in perovskite films. Finally, being able to control these and other defect concentrations is paramount for allowing perovskite optoelectronic devices to reach their radiative limit.

Conflicts of interest

There are no conflicts to declare.

Acknowledgements

This work received partial support from the Office of Naval Research (ONR) Young Investigator Program (Award #N00014-17-1-2005). This work was also supported by ExxonMobil through its membership in the Princeton E-filliates Partnership of the Andlinger Center for Energy and the Environment. P. S. was supported by the HPSC Program funded by U.S. Department of Energy (DOE) Solar Energy Technology Office (SETO) and J. J. B. was supported by the U.S. Office of Naval Research both under DOE Contract Number DE-AC36-08-GO28308 with NREL. P. S. additionally thanks the French Agence Nationale de la Recherche for support under the contract number ANR-17-MPGA-0012.

References

1 N. K. Noel, M. Congiu, A. J. Ramadan, S. Fearn, D. P. McMeekin, J. B. Patel, M. B. Johnston, B. Wenger and H. J. Snaith, *Joule*, 2017, **1**, 328–343.
2 Z. Liu, J. Hu, H. Jiao, L. Li, G. Zheng, Y. Chen, Y. Huang, Q. Zhang, C. Shen, Q. Chen and H. Zhou, *Adv. Mater.*, 2017, **29**, 1606774.
3 R. Brenes, D. Guo, A. Osherov, N. K. Noel, C. Eames, E. M. Hutter, S. K. Pathak, F. Niroui, R. H. Friend, M. S. Islam, H. J. Snaith, V. Bulović, T. J. Savenije and S. D. Stranks, *Joule*, 2017, **1**, 155–167.
4 Z. Xiao, R. A. Kerner, L. Zhao, N. L. Tran, K. M. Lee, T.-W. Koh, G. D. Scholes and B. P. Rand, *Nat. Photonics*, 2017, **11**, 108–115.
5 Y. Jia, R. A. Kerner, A. J. Grede, B. P. Rand and N. C. Giebink, *Nat. Photonics*, 2017, **11**, 784–788.
6 H.-H. Fang, S. Adjokatse, H. Wei, J. Yang, G. R. Blake, J. Huang, J. Even and M. A. Loi, *Sci. Adv.*, 2016, **2**, e1600534.
7 M. A. Green, Y. Hishikawa, E. D. Dunlop, D. H. Levi, J. Hohl-Ebinger and A. W. Y. Ho-Baillie, *Prog. Photovolt. Res. Appl.*, 2018, **26**, 3–12.
8 S. Rühle, *Sol. Energy*, 2016, **130**, 139–147.
9 R. A. Kerner, T. H. Schloemer, P. Schulz, J. J. Berry, J. Schwartz, A. Sellinger and B. P. Rand, *J. Mater. Chem. C*, 2018, DOI: 10.1039/c8tc04871a.
10 Z. Zhou, Z. Wang, Y. Zhou, S. Pang, D. Wang, H. Xu, Z. Liu, N. P. Padture and G. Cui, *Angew. Chem., Int. Ed.*, 2015, **54**, 9705–9709.
11 N. K. Noel, S. N. Habisreutinger, B. Wenger, M. T. Klug, M. T. Hörantner, M. B. Johnston, R. J. Nicholas, D. T. Moore and H. J. Snaith, *Energy Environ. Sci.*, 2017, **10**, 145–152.
12 S. Lee, J. H. Park, B. R. Lee, E. D. Jung, J. C. Yu, D. Di Nuzzo, R. H. Friend and M. H. Song, *J. Phys. Chem. Lett.*, 2017, **8**, 1784–1792.
13 Y. Lin, Y. Bai, Y. Fang, Z. Chen, S. Yang, X. Zheng, S. Tang, Y. Liu, J. Zhao and J. Huang, *J. Phys. Chem. Lett.*, 2018, **9**, 654–658.
14 H. Zhang, X. Ren, X. Chen, J. Mao, J. Cheng, Y. Zhao, Y. Liu, J. Milic, W.-J. Yin, M. Grätzel and W. C. H. Choy, *Energy Environ. Sci.*, 2018, **11**, 2253–2262.
15 A. J. Ramadan, N. K. Noel, S. Fearn, N. Young, M. Walker, L. A. Rochford and H. J. Snaith., *Chem. Mater.*, 2018, **30**, 7737–7743.
16 K. X. Steirer, P. Schulz, G. Teeter, V. Stevanovic, M. Yang, K. Zhu and J. J. Berry, *ACS Energy Lett.*, 2016, **1**, 360–366.
17 F.-S. Zu, P. Amsalem, I. Salzmann, R.-B. Wang, M. Ralaiarisoa, S. Kowarik, S. Duhm and N. Koch, *Adv. Opt. Mater.*, 2017, **5**, 1700139.
18 Y. Li, X. Xu, C. Wang, B. Ecker, J. Yang, J. Huang and Y. Gao, *J. Phys. Chem. C*, 2017, **121**, 3904–3910.
19 N. H. Nickel, F. Lang, V. V. Brus, O. Shargaieva and J. Rappich, *Adv. Electron. Mater.*, 2017, **3**, 1700158.
20 E. J. Juarez-Perez, Z. Hawash, S. R. Raga, L. K. Ono and Y. Qi, *Energy Environ. Sci.*, 2016, **9**, 3406–3410.
21 R. I. Dawood, A. J. Forty and M. R. Tubbs, *Proc. R. Soc. London, Ser. A*, 1965, **284**, 272–288.
22 M. R. Tubbs, *Proc. R. Soc. London, Ser. A*, 1964, **280**, 566–585.
23 A. J. Forty, *Philos. Mag.*, 1961, **6**, 895–905.
24 M. L. Agiorgousis, Y.-Y. Sun, H. Zeng and S. Zhang, *J. Am. Chem. Soc.*, 2014, **136**, 14570–14575.
25 I. A. Shkrob and T. W. Marin, *J. Phys. Chem. Lett.*, 2014, **5**, 1066–1071.
26 S. D. Stranks, V. M. Burlakov, T. Leijtens, J. M. Ball, A. Goriely and H. J. Snaith, *Phys. Rev. Appl.*, 2014, **2**, 034007.
27 F. Liu, Q. Dong, M. K. Wong, A. B. Djurišić, A. Ng, Z. Ren, Q. Shen, C. Surya, W. K. Chan, J. Wang, A. M. C. Ng, C. Liao, H. Li, K. Shih, C. Wei, H. Su and J. Dai, *Adv. Energy Mater.*, 2016, **6**, 1502206.
28 F. Wang, H. Yu, H. Xu and N. Zhao, *Adv. Funct. Mater.*, 2015, **25**, 1120–1126.
29 G. Sadoughi, D. E. Starr, E. Handick, S. D. Stranks, M. Gorgoi, R. G. Wilks, M. Bär and H. J. Snaith, *ACS Appl. Mater. Interfaces*, 2015, **7**, 13440–13444.